

LEVEL #

(12)
#

Microwave SQUID A/D Converters

A. H. SILVER, J. P. HURRELL, and Y. SONG
Electronics Research Laboratory
D. C. PRIDMORE-BROWN
Space Sciences Laboratory
Laboratory Operations
The Aerospace Corporation
El Segundo, Calif. 90245

5 June 1980

Interim Report

APPROVED FOR PUBLIC RELEASE;
DISTRIBUTION UNLIMITED

DTIC
ELECTE
JUN 24 1980
A

Prepared for
OFFICE OF NAVAL RESEARCH
Washington, D.C. 22217

SPACE DIVISION
AIR FORCE SYSTEMS COMMAND
Los Angeles Air Force Station
P.O. Box 92960, Worldway Postal Center
Los Angeles, Calif. 90009

80

6 23 012

ADA 085897

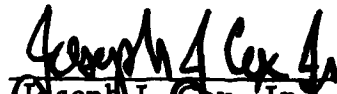
DDC FILE COPY

This interim report was submitted by The Aerospace Corporation, El Segundo, CA 90245, under Contract No. F04701-79-C-0080 with the Space Division, Deputy for Technology, P. O. Box 92960, Worldway Postal Center, Los Angeles, CA 90009. It was reviewed and approved for The Aerospace Corporation by M. T. Weiss, Vice President and General Manager, Laboratory Operations. Lieutenant James C. Garcia, SD/YLXT, was the project officer for Technology.

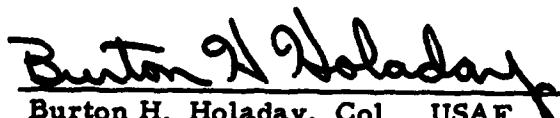
This report has been reviewed by the Public Affairs Office (PAS) and is releasable to the National Technical Information Service (NTIS). At NTIS, it will be available to the general public, including foreign nations.

This technical report has been reviewed and is approved for publication. Publication of this report does not constitute Air Force approval of the report's findings or conclusions. It is published only for the exchange and stimulation of ideas.


James C. Garcia, Lt, USAF
Project Officer


Joseph J. Cox, Jr., Lt. Col.
USAF
Chief, Advanced Technology
Division

FOR THE COMMANDER


Burton H. Holaday, Col., USAF
Director of Technology Plans and
Analysis
Deputy for Technology

UNCLASSIFIED

SECURITY CLASSIFICATION OF THIS PAGE (When Data Entered)

19 REPORT DOCUMENTATION PAGE		READ INSTRUCTIONS BEFORE COMPLETING FORM	
1. REPORT NUMBER SD-TR-80-34	2. GOVT ACCESSION NO. AD-A085897	3. RECIPIENT'S CATALOG NUMBER	
4. TITLE (and Subtitle) MICROWAVE SQUID A/D CONVERTERS,		5. TYPE OF REPORT & PERIOD COVERED Interim Technical Repts	
7. AUTHOR(s) Arnold H. Silver, John P. Hurrell, Yeong-Du Song, David Pridmore-Brown		6. PERFORMING ORG. REPORT NUMBER TR-0080(5732)-1	
9. PERFORMING ORGANIZATION NAME AND ADDRESS The Aerospace Corporation El Segundo, Calif. 90245		8. CONTRACT OR GRANT NUMBER(s) F04701-79-C-0080	
11. CONTROLLING OFFICE NAME AND ADDRESS Office of Naval Research Washington, D. C. 22217		10. PROGRAM ELEMENT, PROJECT, TASK AREA & WORK UNIT NUMBERS 12, 36	
14. MONITORING AGENCY NAME & ADDRESS (if different from Controlling Office) Space Division Air Force Systems Command Los Angeles, Calif. 90009		12. REPORT DATE 5 Jun 80	
		13. NUMBER OF PAGES 32	
		15. SECURITY CLASS. (of this report) Unclassified	
		15a. DECLASSIFICATION/DOWNGRADING SCHEDULE	
16. DISTRIBUTION STATEMENT (of this Report) Approved for public release; distribution unlimited			
17. DISTRIBUTION STATEMENT (of the abstract entered in Block 20, if different from Report)			
18. SUPPLEMENTARY NOTES			
19. KEY WORDS (Continue on reverse side if necessary and identify by block number) Josephson junctions SQUIDS Analog-to-digital converter Scaler			
20. ABSTRACT (Continue on reverse side if necessary and identify by block number) This document reports progress on the demonstration of an analog-to-digital converter using Josephson junction SQUID circuits. The projected performance envisions an aperture time limit of 0.25×10^{-12} sec with the Pb alloy junction technology. The status of junction fabrication and circuit simulations are reported. times 16 to 12			

DD FORM 1473
(FACSIMILE)UNCLASSIFIED 009573
SECURITY CLASSIFICATION OF THIS PAGE (When Data Entered)

SUMMARY

We have developed sufficient technology to make superconducting microwave integrated circuits with four active elements. This has enabled us to fabricate pairs of coupled scalar cells and study their free-running performance at high frequencies. Coupling between a first cell running at 15 GHz and a second at 7.5 GHz has been demonstrated and continues to be actively investigated. Also we have developed the necessary computer programs and successfully performed a comprehensive simulation of analog/digital (A/D) conversion, and have established criteria for the microwave design. An ultimate response time of 0.25 ps has been predicted for sufficiently small devices, leading to picosecond aperture times per bit.

Distribution for 1. <input type="checkbox"/> General 2. <input type="checkbox"/> Field 3. <input type="checkbox"/> Requested 4. <input type="checkbox"/> Information	
Distribution/	
Availability Codes	
Dist A	Avail and/or special

PREFACE

This work was supported in part by The Aerospace Corporation under an Aerospace-sponsored research program.

CONTENTS

SUMMARY	1
PREFACE	3
INTRODUCTION	9
PROGRESS	11
Fabrication	11
Performance of Coupled Scaler Cells	16
Simulation	19
Design Considerations	34

FIGURES

1.	(a) General View of Sapphire Substrate. (b) Photomicrograph of a Coupled Pair of dc SQUIDs	12
2.	Critical Current Density vs Oxidation Time	13
3.	(a) Photomicrograph of 5 μm Diode. (b) Scanning Electron Micrograph of 2.5 μm Diode	15
4.	Electrical Circuit of Two Coupled Scaler Cells	17
5.	Current vs Voltage Curves for the Circuit Shown in Fig. 4	18
6.	Circuit for Simulation of A/D Conversion	20
7.	Pulse Shape for Single Cell with Three Values of Capacitance ($\epsilon \equiv R^2 C/L$) and $\beta = \pi$, $I_0 = 0.85 I_c$	25
8.	Pulse Shape for Single Cell with Three Values of Propagation Delay (2τ) Between Junctions and $\epsilon = 0.25$, $\beta = \pi$, $I_0 = 0.85 I_c$	27
9.	Simulation of Converter Response with Quantizer and Two Scaler Cells	28
10.	Simulation of Converter Response with Nominal Circuit Parameters Except that $\tau_x = 5$	29
11.	Simulation Same as in Fig. 9	30
12.	Simulation Same as in Fig. 9 Except that a Fast Ramp is Used ($\dot{I} = 2.5 I_c R/L$)	31
13.	Simulation Same as in Fig. 12	32
14.	Simulation to Demonstrate Ultimate Performance	35
15.	Design Parameters for a Critically Damped SQUID with β -Value of π	36

INTRODUCTION

In 1978, we introduced a concept for the front end of a high speed superconducting A/D converter.¹ The analog signal is applied to a single-junction SQUID and converted into a pulse train resulting from fluxoid transitions. These are counted in a chain of bistable dc SQUIDs that successively scale the pulse train by a factor 2. The bit count stored in the array is gated out in parallel, with each sampling interval being used to provide the digitized signal. These SQUIDs would be performing both logic and memory functions at the single fluxoid level.

We have concentrated our attention on two aspects of this device in FY 79: performance simulation and demonstration of high speed scaling. The performance has been simulated on a computer, and criteria established for the microwave SQUID design. These criteria include dimensionality, impedance, damping, β -factor, and both inter- and intra-SQUID delays. Rather than trying to demonstrate scaling directly, we chose to pursue subharmonic frequency locking between SQUIDs. Two coupled dc SQUIDs were fabricated, the first to generate and self-detect frequencies near 15 GHz, and the second to operate at 7.5 GHz.

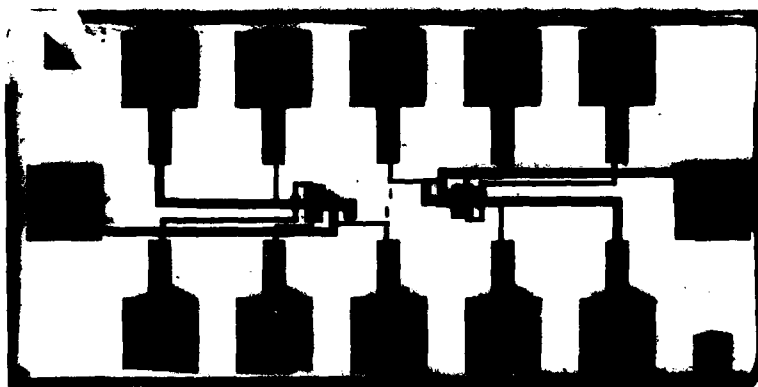
¹J. P. Hurrell and A. H. Silver, "SQUID Digital Electronics," Future Trends in Superconductive Electronics, Vol. 44, American Institute of Physics, New York (1978), p. 437.

PROGRESS

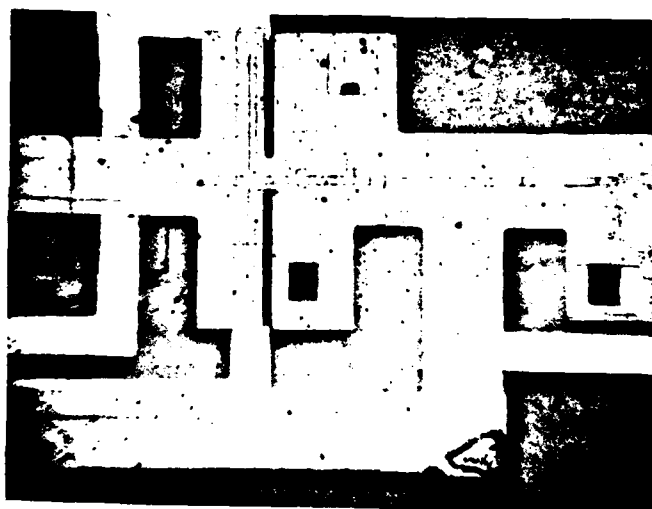
FABRICATION

We have used the lead/indium alloy technology developed by IBM to fabricate Josephson tunnel junctions that are integrated with microstrip transmission lines composed of the same alloys with a SiO dielectric spacer. We have not used a separate ground plane, and consequently all devices – namely diodes, resistors, and coupling transformers – are essentially sandwiched between the two conductors.

The devices are fabricated on a polished sapphire substrate with dimensions of 1 x 0.5 x 0.025 in. A typical wafer can be seen in Fig. 1(a). Two identical circuits have been constructed and connected to a contact pad array. Figure 1(b) is a photomicrograph of one of these circuits, used to investigate the performance of a pair of coupled dc SQUIDs. Thin film resistors, composed from a gold/palladium alloy, are first evaporated and patterned. The first base-electrode of a pair of coupled SQUIDs is then deposited. Approximately 200 Å of indium, followed by 2000 Å of lead, is evaporated and patterned with a "lift-off" stencil formed from Shipley photoresist soaked in chlorobenzene. Next the first transformer dielectric spacer is deposited. The SiO is evaporated at less than 10 Å/s in a vacuum of 10^{-6} Torr and is patterned in the same manner. Then the second base-electrode of the pair and the microstrip spacer are deposited. Windows are left for the tunnel junctions and for contact to the resistors. The tunnel junction oxide is grown in radio-frequency (rf) plasma glow discharge, following a sputter cleaning. The log current density is inversely proportional to the oxidation time, as shown in Fig. 2. About 4 W of rf is applied to an 8-in. electrode in an oxygen atmosphere at 20 m Torr. Finally, the top electrode, which is also the ground plane for the microstrip, is deposited. Typically 5000 Å of pure lead is used.



(a)



(b)

Fig. 1. (a) General View of Sapphire Substrate.
(b) Photomicrograph of a Coupled Pair of dc SQUIDs.

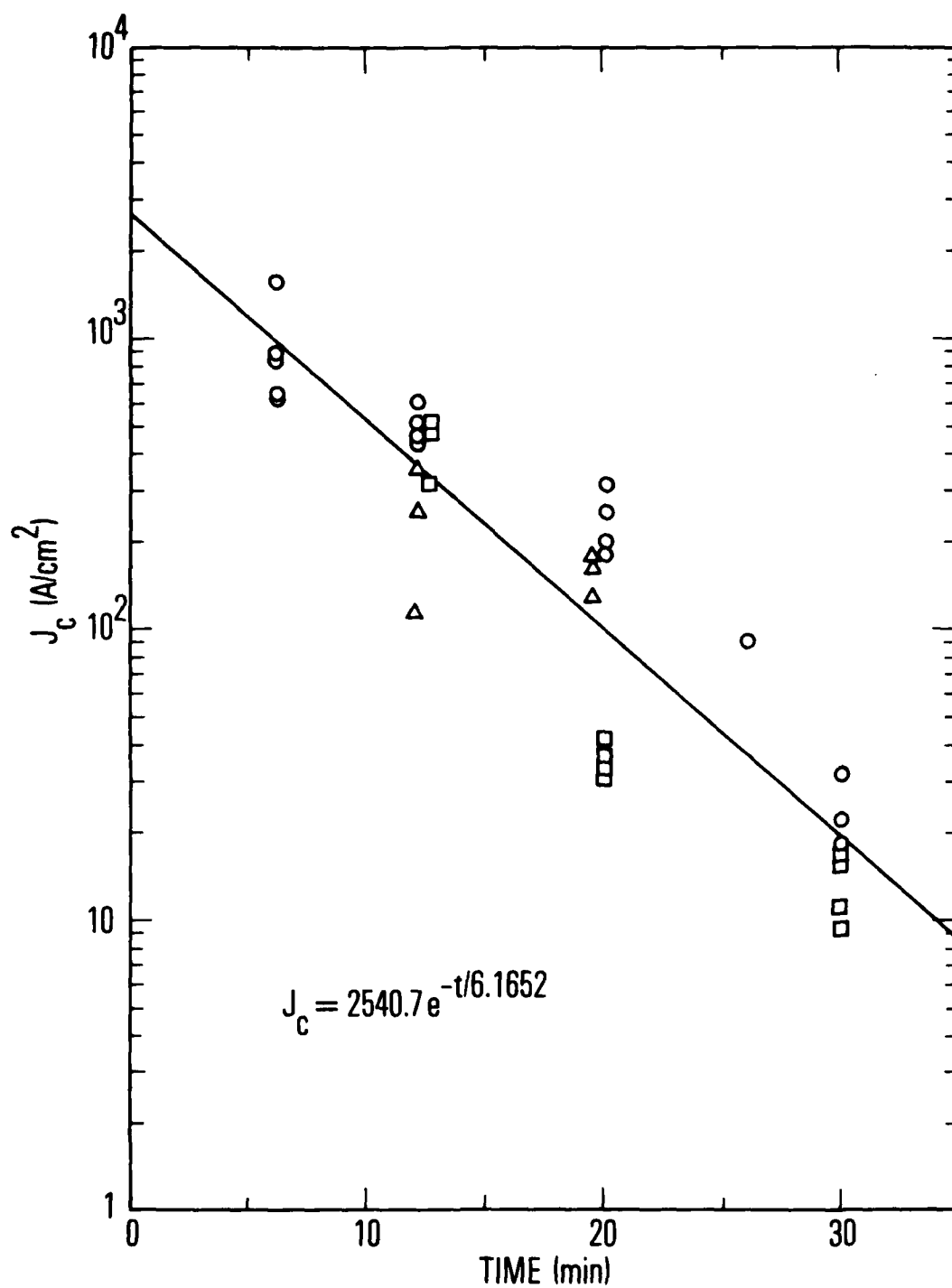
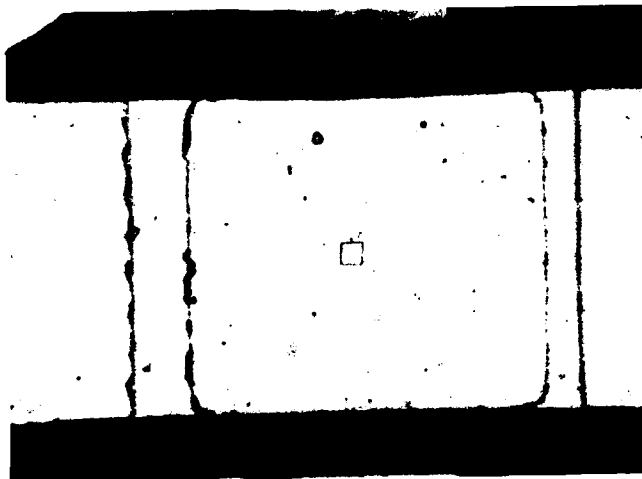


Fig. 2. Critical Current Density vs Oxidation Time. Individual points show both the variation from run to run and the variation on the substrates.

All metal evaporations are carried out at 10^{-6} Torr in a vacuum system evacuated by a 6-in. diffusion pump, baffled by a liquid nitrogen cold trap. A multiple source, Temescal e-gun is used to evaporate the metals. The SiO is evaporated from a resistively heated baffle box. Radio-frequency sputter cleaning is performed prior to all depositions to improve film adhesion.

The minimum linewidth being used in this photoresist technology is 20 μm . Whereas this can comfortably be reduced with higher resolution masks, ultimate goals for high speed require submicron dimensions. These can be achieved only by special photoresist techniques or by electron lithography. Consequently, the use of an electron resist to pattern small diodes is being investigated. We have fabricated SiO windows via "lift-off" with polymethylmethacrylate stencils down to 1- μm dimension. Figure 3(a) is a photomicrograph that shows the general layout for a 5- μm diode, and Fig. 3(b) is a scanning electron microscope (SEM) picture of the top of a 2.5- μm diode. Our current yield of devices with these small dimensions is low, and we do not anticipate that consistent, smaller devices can be easily achieved with this geometry.

Also we are attempting to emulate more closely the IBM technology. In particular, we are depositing niobium ground planes on silicon wafers, and are fabricating diodes with the sputter oxidation process. Neither the yield nor the quality of their I-V curves has consistently approached those of the glow-discharge fabricated diodes, as yet.



(a)



(b)

Fig. 3. (a) Photomicrograph of 5 μm Diode.
(b) Scanning Electron Micrograph of 2.5 μm Diode

PERFORMANCE OF COUPLED SCALER CELLS

We had studied previously the dynamics of circulating currents in dc SQUIDs.² The circulating current reverses its direction in the scaler cell with the application of a short pulse to the center of the SQUID, and an associated voltage pulse is detected alternately at each junction. If the SQUID is underdamped, current steps can occur in its I-V curve when the internal LC resonance is excited at half-integral flux bias. This implies that the SQUID can operate as an oscillator and self-detector at the same time. Consequently, we have used a dc SQUID as a source of microwave current in the vicinity of its LC resonant frequency, and have applied this current to the center of a second similar dc SQUID. By monitoring the performance of this second SQUID, we are able to ascertain whether appropriate coupling and subharmonic phase locking has been achieved. In particular, the LC resonance in the second SQUID is selected to be at the same frequency as that in the first. Then a resonance step induced at half this frequency results from the scaling action or frequency division envisaged in the A/D converter.

The electrical circuit is shown in Fig. 4. Transformer coupling between SQUIDs should ensure dc isolation. The circuit has not been optimized, and external inductances that are comparable to those of the SQUIDs remain. Nevertheless, adequate coupling should exist for the second SQUID to be driven by the first. The SQUID parameters are similar to those reported previously.² Figure 5 shows the two I-V curves for a particular run. Curve V_1 exhibits the resonance step of SQUID 1 at approximately 30 μ V, implying a frequency of 15 GHz. Curve V_2 exhibits two resonance steps, one at about 30 μ V (its own resonance) and a second step at approximately 15 μ V, implying an enhanced circulating current component at 7.5 GHz. The dotted line traces the I-V curve for the second SQUID with integral flux bias, showing the expected absence of any resonances. Conclusive demonstration of this proposed phase locking at subharmonic frequencies is marred by a ubiquitous, quasi dc coupling between the SQUIDs that directly couples their I-V curves. This problem is currently under investigation.

²Y. Song and J. P. Hurrell, "LC Resonance Steps in the I-V Characteristics of dc SQUIDs," IEEE Trans. Mag. **15**, 428 (1979).

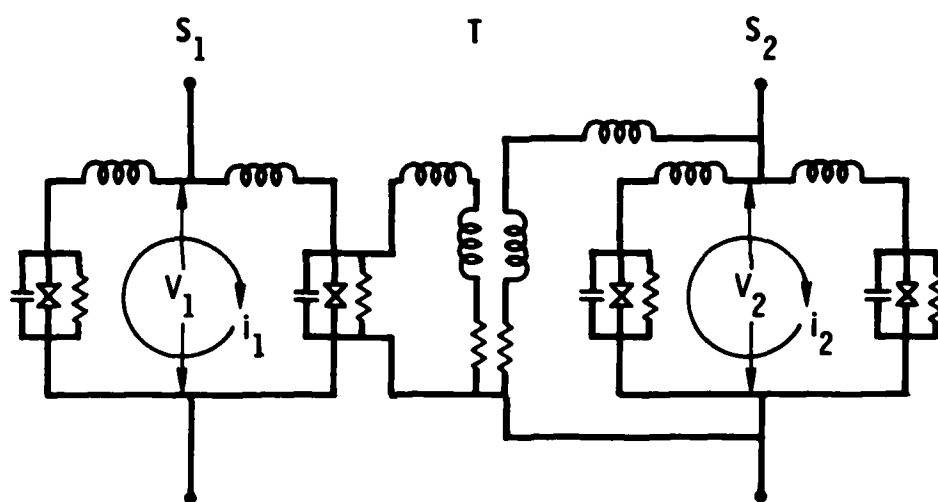


Fig. 4. Electrical Circuit of Two Coupled Scalar Cells

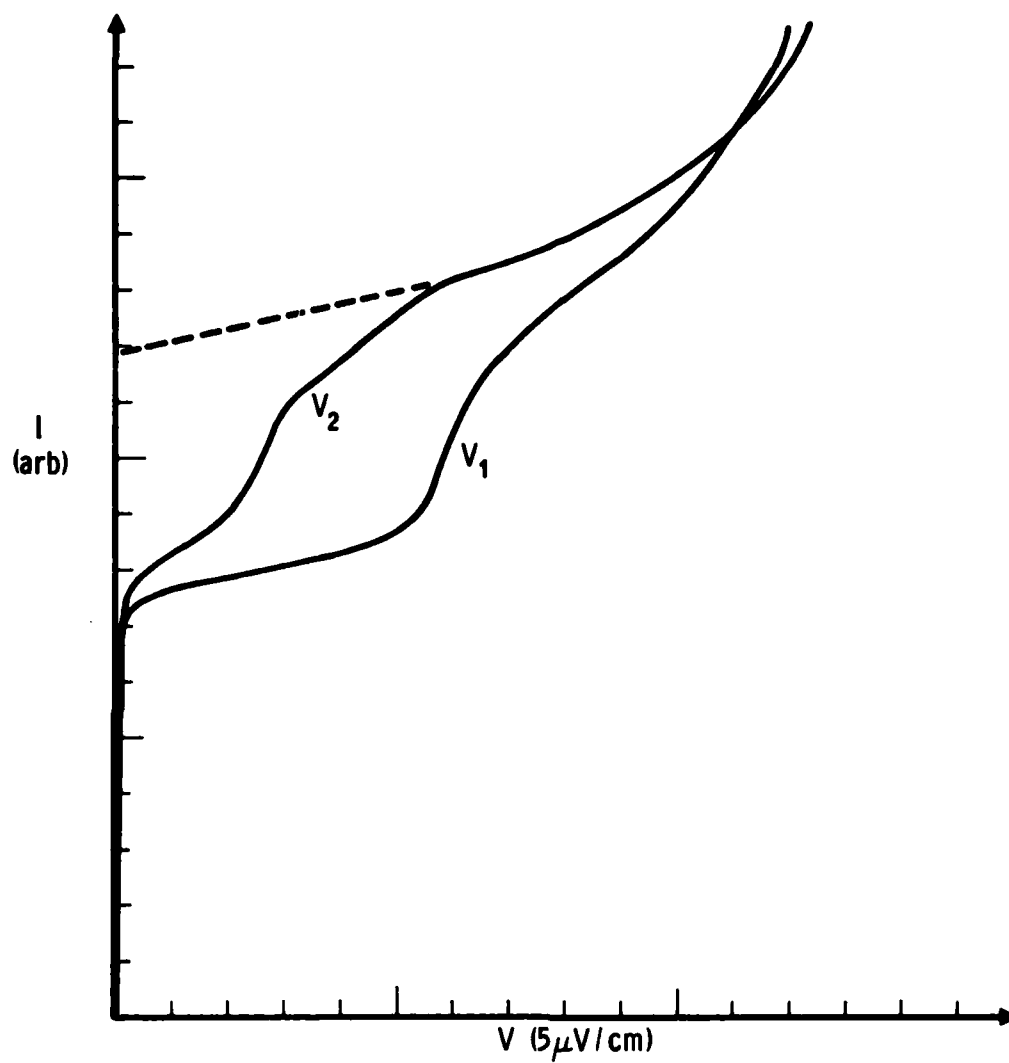


Fig. 5. Current vs Voltage Curves for the Circuit Shown in Fig. 4

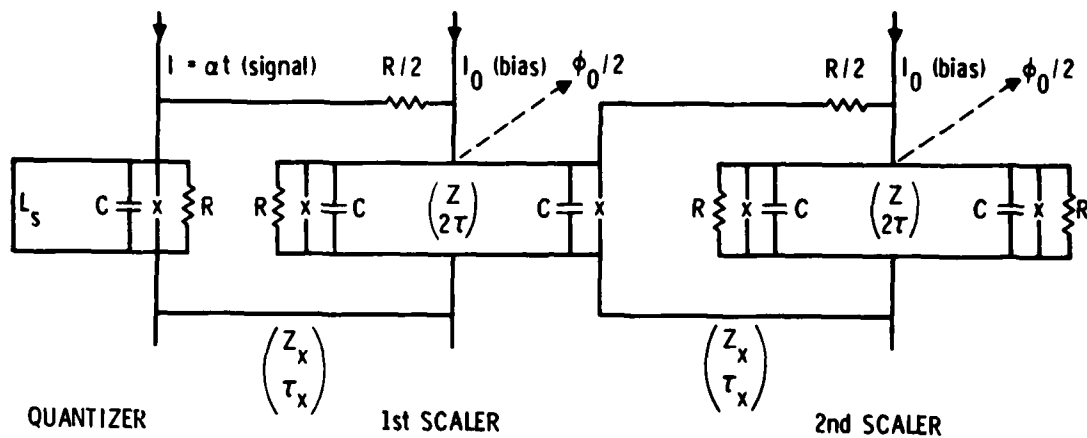
SIMULATION

We have extended our simulation of the performance of this A/D converter by studying the behavior of an SJ-SQUID coupled to an array of two or more DJ-SQUIDS via microstrip transmission lines.

Junction performance is represented by a tunneling current $I_c \sin \theta + G(\theta)V$ and a displacement current $C\dot{V}$. I_c is the junction critical current, $V = (\phi_0/2\pi)\dot{\theta}$ is the junction voltage, θ is the superconducting phase difference across the junction, C is the capacitance of the junction, and $G(\theta)$ represents quasiparticle tunneling effects. $G(\theta)$ may be safely ignored in the presence of loading impedances R , Z_x as long as frequencies remain far below the gap frequency. This point will be considered later when the issue of ultimate speed is addressed. At microwave frequencies, small lumped inductances become difficult to use and microstrip is usually substituted. This may lead to propagation delay effects, which can be included in the calculation by allowing a microstrip impedance Z and propagation delay 2τ . The design issues that arise from the effects of both C and τ will be discussed in a later section. The microstrip coupling between SQUIDS is represented by impedances Z_x and propagation delays of τ_x . A series resistance $R/2$ is included (as shown in Fig. 6) to provide some additional damping and matching. In general Z and Z_x are not equal, and parasitic inductances may exist between the tunnel junctions and the microstrips; they are not included in the calculations.

Circuit simulations require a set of integrable equations that describe the performance of these junctions in the microwave circuits. Rather than use standard computer programs, we chose to derive the circuit equations and integrate them directly. Two types of transmission lines have to be considered, namely, the interconnection between SQUIDS and the intraconnection between junctions in the DJ-SQUID. Different, but equivalent, sets of equations are used for the two types of connections.

The interconnection between SQUIDS requires that the input to the first SQUID be transformed from the output of the second and vice versa



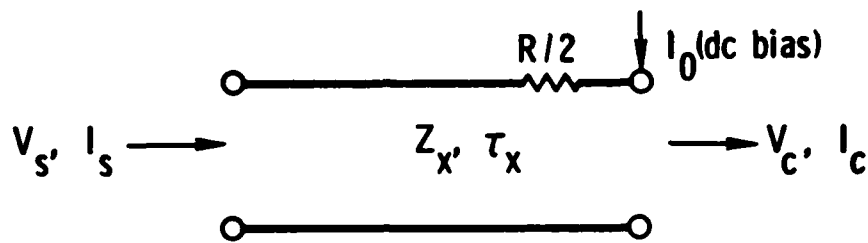
NOMINAL VALUES $\tau = 1/4 (L/R)$; $\tau_x = 1/2 (L/R)$; $Z_x = R$

$$I_c (\text{quantizer}) = \sqrt{2} I_c (\text{scaler})$$

$$\sqrt{2} L_s = L (\text{scaler}) \equiv 2 L$$

ALL β -VALUES = π

Fig. 6. Circuit for Simulation of A/D Conversion



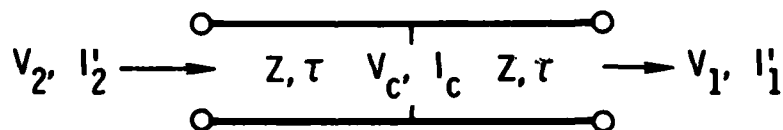
$$V_s(t) - Z_x I_s(t) = V_c(t - \tau_x) + (R/2 - Z_x) \{I_c(t - \tau_x) - I_0\} \quad (1)$$

$$\equiv -Z_x I_x(t - \tau_x)$$

and

$$V_c(t) = Z_x I_x(t - 2\tau_x) + 2V_s(t - \tau_x) - (R/2 + Z_x) \{I_c(t) - I_0\} \quad (2)$$

The intraconnection in the DJ-SQUID transforms the input V_c, I_c to the two junctions as follows



$$Z I_c(t) = Z I_c(t - 2\tau) + 2 \{V_c(t) + V_c(t - 2\tau) - V_1(t - \tau) - V_2(t - \tau)\} \quad (3)$$

and

$$V_j(t) + Z I_j'(t) = V_j(t - 2\tau) + Z I_j'(t - 2\tau) + 2 \{V_c(t - \tau) - V_j(t - 2\tau)\} \quad (4)$$

with $j = 1, 2$ representing the right- and left-hand junctions, respectively.

The inductance L_s of the quantizer module shown in Fig. 6 was assumed to be a lumped impedance. Then the single node equation, transformed by Eq. (1) becomes

$$C\dot{V}_s(t) + (R^{-1} + Z_x^{-1}) V_s(t) = I(t) - L_s^{-1} \left[\phi_{xs} + \phi_0/2\pi \theta_s(t) \right] - I_{cs} \sin \theta_s(t) - I_x(t - \tau_x) \quad (5)$$

with

$$(\phi_0/2\pi) \dot{\theta}_s(t) = V_s(t) \quad (6)$$

Symbolically these equations transform $I(t)$, $I_x(t - \tau_x)$ into $V_s(t)$. In order to integrate these equations, we assume $I(t) = 0$ for $t < 0$ and at $t = 0$ the quantizer resides in the stationary state defined by

$$L_s I_{cs} \sin \theta_s(0) + \phi_{xs} + (\phi_0/2\pi) \theta_s(0) = 0 \quad (7)$$

Since $I_x(t) = 0$ for $t < \tau_x$, the equations can be integrated immediately up to $t = 2\tau_x$.

Junction equations for the first scaler module may be written in similar fashion using Eq. (1)

$$C\dot{V}_1(t) + (Z^{-1} + Z_x^{-1}) V_1(t) = I_1(t) - I_c \sin \theta_1(t) - \bar{I}_x(t - \tau_x) \quad (8)$$

$$C\dot{V}_2(t) + (Z^{-1} + R^{-1}) V_2(t) = I_2(t) - I_c \sin \theta_2(t) \quad (9)$$

with

$$(\phi_0/2\pi) \dot{\theta}_j(t) = V_j(t), \quad j = 1, 2 \quad (10)$$

Similar equations can be written for succeeding scaler modules. The chain is completed with a matched load, which imposes the condition

$$I_x(t) = (R^{-1} - Z_x^{-1})V_1(t) \quad (17)$$

for the final junction. This forms a closed set of first order differential equations and difference equations for the circuit simulation.

As a preliminary exercise we have pursued the transient response of a single scaler cell; the quantizing cell has received adequate attention in the literature. The transient response of an isolated scaler cell can be evaluated by determining the response to its own output pulse when τ_x is extended until no reflections occur before the pulse is over. In the simulation, we have put $Z_x = R$ and $\beta = \pi$. If the DJ-SQUID inductance $2L$ is determined by fixing the flux quantum energy $\phi_0^2/4L$, the values of Z and τ become related by $L = Z\tau$. Then different values of τ are achieved by choosing different impedances Z .

In the first simulation, shown in Fig. 7, the output voltage has been calculated for different capacitances C , in the limit $\tau \rightarrow 0$; $\epsilon \equiv R^2 C/L$. The absence of capacitance is represented by $\epsilon = 0$; critical damping occurs for $\epsilon = 0.25$, and severe underdamping is simulated by taking $\epsilon = 1$. The curves show that some capacitance can be tolerated in the SQUID without seriously degrading its performance. The shape of the pulse depends on the value of the bias current I_0 , and a value $I_0 = 0.85 I_c$ was chosen. A value of capacitance appropriate to critical damping becomes a natural choice that imposes the least restriction on junction size and current density while maintaining a good performance.

The simulation shown in Fig. 8 was generated with $\epsilon = 0$ and $I_0 = 0.85 I_c$. In this case, finite values of τ have been chosen, resulting in pulse broadening from the distributed capacitance in the microstrip. τ values are written in units of (L/R) , such that $\tau = 1$ occurs for $Z = R$. Remembering that $Z_x = R$, we have $Z = Z_x$ for $\tau = 1$. This corresponds to a design in which the microstrip connecting the SQUIDS is identical to that providing the SQUID

Here $\bar{I}_x(t)$ represents the input from the second scaler module and

$$\begin{aligned} I_j(t) &\equiv Z^{-1}V_j(t) + I_j'(t) \\ &= I_j(t - 2\tau) + 2Z^{-1}\{V_c(t - \tau) - V_j(t - 2\tau)\} \text{ from Eq. (4)} \end{aligned} \quad (11)$$

The equations for the scaler module are completed with the following difference equations for $I_x(t)$ from Eq. (1), and $V_c(t)$, $I_c(t)$ from Eqs. (2) and (3)

$$I_x(t) = (1 - R/2Z_x)(I_c(t) - I_0) - Z_x^{-1}V_c(t) \quad (12)$$

$$\begin{aligned} V_c(t) &= \left[1 + \frac{R + 2Z_x}{Z}\right]^{-1} \left\{ 2V_s(t - \tau_x) + Z_x I_x(t - 2\tau_x) - (R/2 + Z_x) \right. \\ &\quad \left. \left[I_c(t - 2\tau) - I_0 + 2Z^{-1}[V_c(t - 2\tau) - V_1(t - \tau) - V_2(t - \tau)] \right] \right\} \end{aligned} \quad (13)$$

$$I_c(t) = I_c(t - 2\tau) + 2/Z[V_c(t) + V_c(t - 2\tau) - V_1(t - \tau) - V_2(t - \tau)] \quad (14)$$

Symbolically these equations transform $V_s(t - \tau_x)$, $\bar{I}_x(t - \tau_x)$ into $V_1(t)$, $I_x(t)$. Clearly the integration can now be carried out up to $t = 3\tau_x + \tau$. Initial states at $t = 0$ are defined by

$$I_0 = I_c[\sin \theta_1(0) + \sin \theta_2(0)] \quad (15)$$

$$Z\tau I_c[\sin \theta_1(0) - \sin \theta_2(0)] \pm \phi_0/2 + (\phi_0/2\pi)[\theta_1(0) - \theta_2(0)] = 0 \quad (16)$$

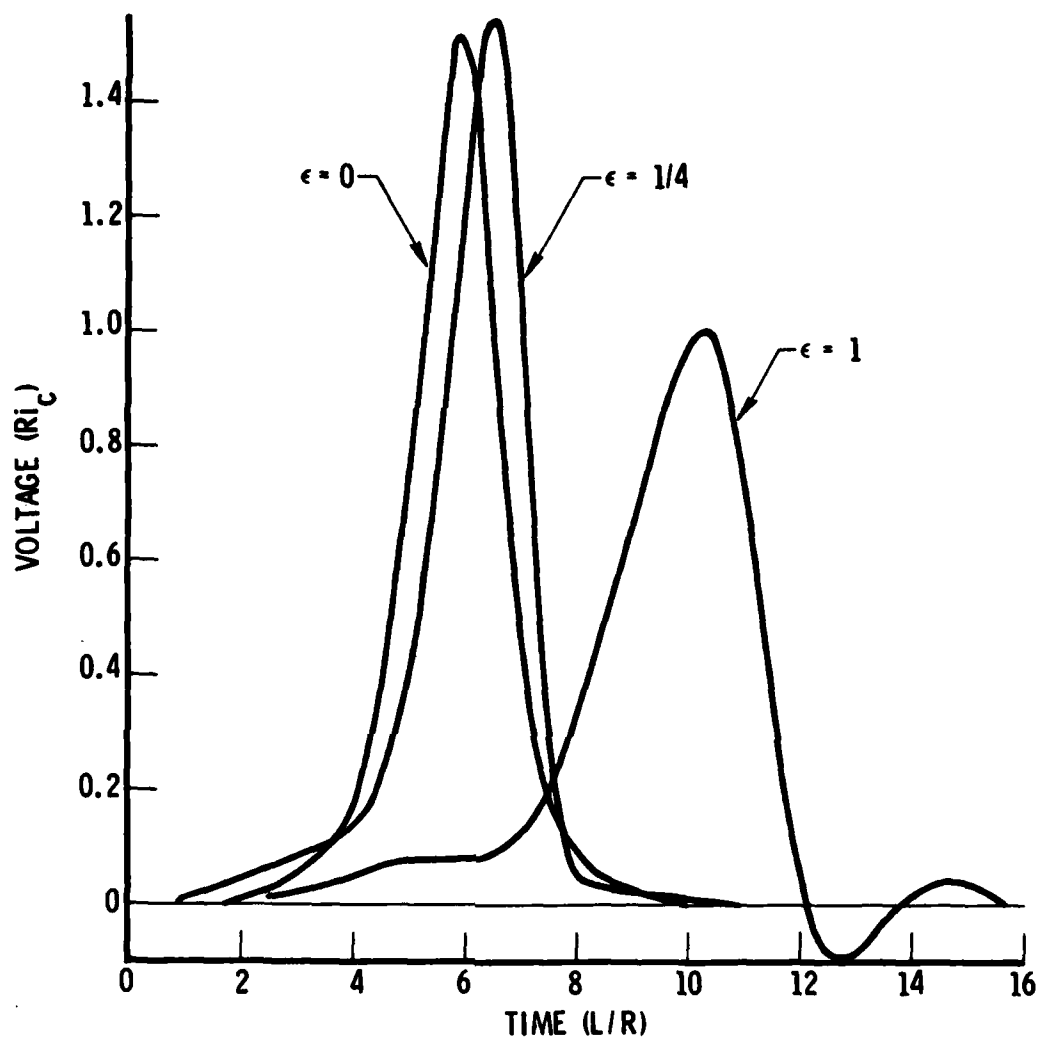


Fig. 7. Pulse Shape for Single Cell with Three Values of Capacitance ($\epsilon \equiv R^2 C/L$) and $\beta = \pi$, $I_0 = 0.85 I_c$

inductance. A value of $\tau < 0.25$ appears to be necessary to prevent excessive broadening and delay. This imposes an impedance requirement of $Z > 4Z_x$.

These guidelines have been imposed on the complete simulation of A/D conversion. Nominal values for the scaler cells become $\tau = 0.25(L/R)$, $Z_x = R$, $\epsilon = 0.25$ and $\beta = \pi$. The quantizer cell was also chosen with a β value of π , but delay effects were neglected with $\tau = 0$. The choice of inductance $L_s = \sqrt{2}L$ was made to minimize some of the effects resulting from the differences between the SJ-SQUID and the DJ-SQUID, but this choice does not strongly affect the results.

A nominal converter response is shown in Fig. 9. This has been derived for a ramp signal $\dot{I} = I_c R/10L$, terminated and maintained at constant value after the quantizer had been driven through three levels. The value $\tau_x = 0.5(L/R)$ was selected to maintain a propagation delay between SQUIDs, yet to remain close to lumped performance so that the full consequences of mutual reflections among the cells could be exhibited. Two scaler cells were included and the bar quantities refer to the second scaler. In the first event, the quantizer drives the first scaler, which in turn drives the second scaler corresponding to the bit change $(11) \rightarrow (00)$. The excessive ringing of V_1 as compared to \bar{V}_1 illustrates the need for more damping between scaler cells. A similar improvement in the ringing is achieved by increasing the value of τ_x and delaying the reflected pulses, as seen in Fig. 10, where two level changes have been simulated with a similar ramp input. The second event in Fig. 9 switches only the first scaler corresponding to $(00) \rightarrow (10)$. The third event mirrors the first with $(10) \rightarrow (01)$.

Figure 11 displays the same events of Fig. 9 in terms of junction phases evolving with time. The signal curve merely shows the quantizer drive. If the ramp speed is increased the quantizer switches faster, as do the scaler cells, but delays are incurred because the SQUIDs tend to respond with their natural (L/R) times. Figures 12 and 13 demonstrate this response for $\dot{I} = 2.5 I_c (R/L)$. Even at this speed, the converter will maintain correct scaling action as long as the ramp level is maintained at the end of the sweep.

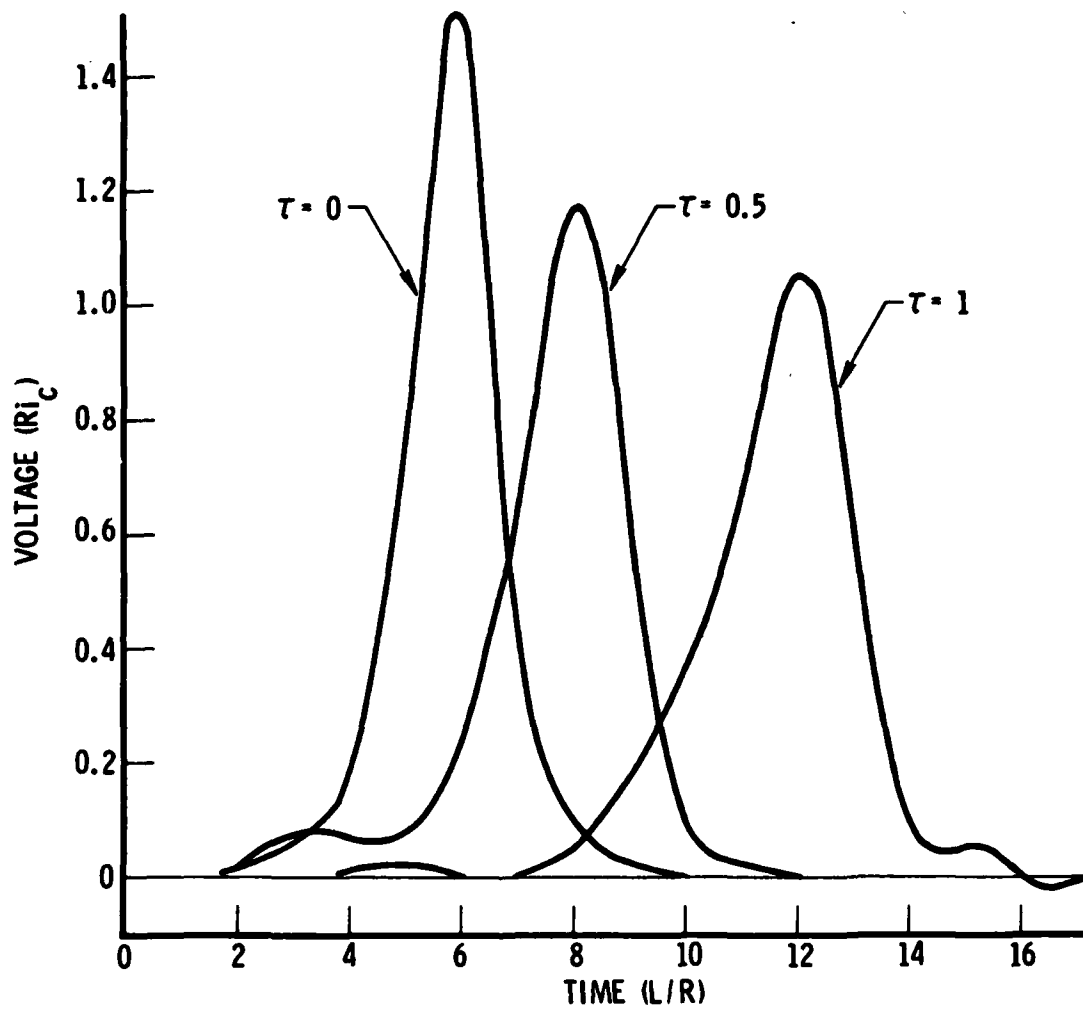


Fig. 8. Pulse Shape for Single Cell with Three Values of Propagation Delay (2τ) Between Junctions and $\epsilon = 0.25$, $\beta = \pi$, $I_0 = 0.85 I_c$

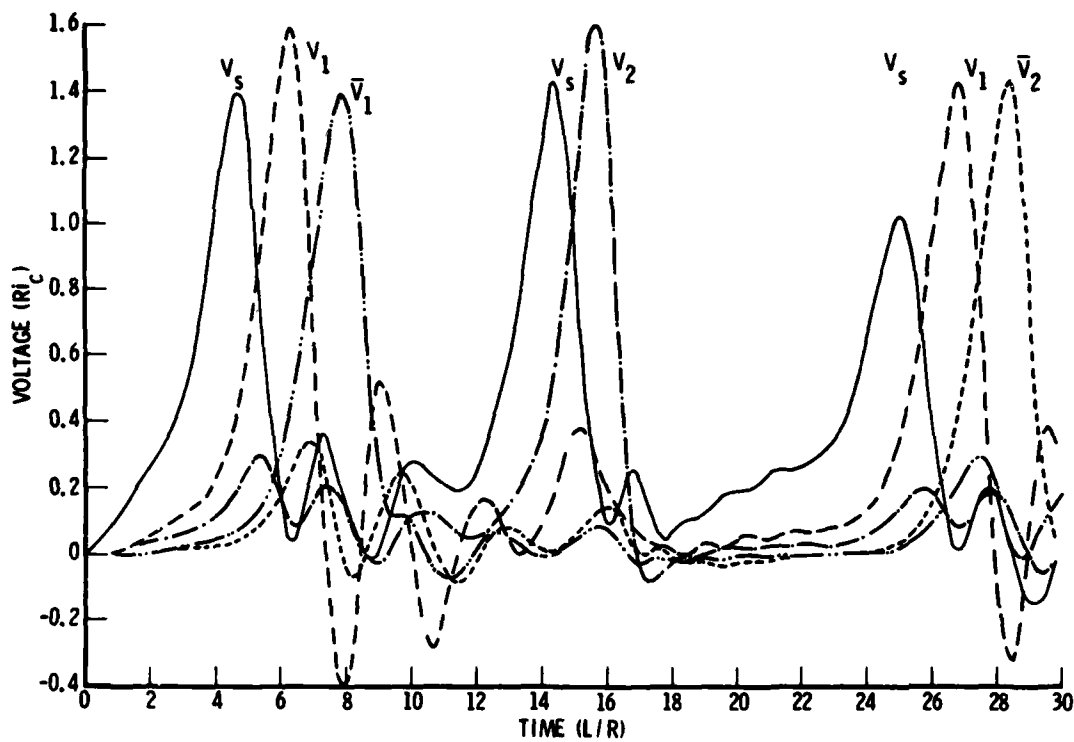


Fig. 9. Simulation of Converter Response with Quantizer and Two Scaler Cells. Nominal values are shown in Fig. 6 for circuit parameters.

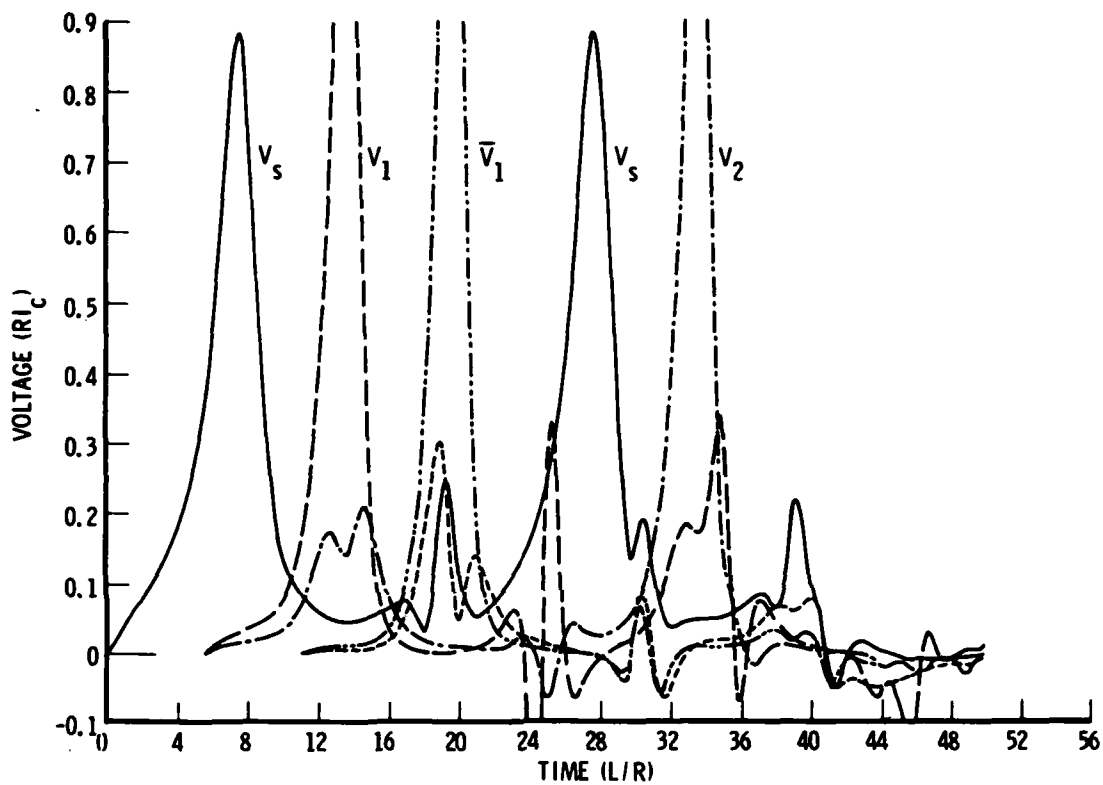


Fig. 10. Simulation of Converter Response with Nominal Circuit Parameters Except That $\tau_x = 5$

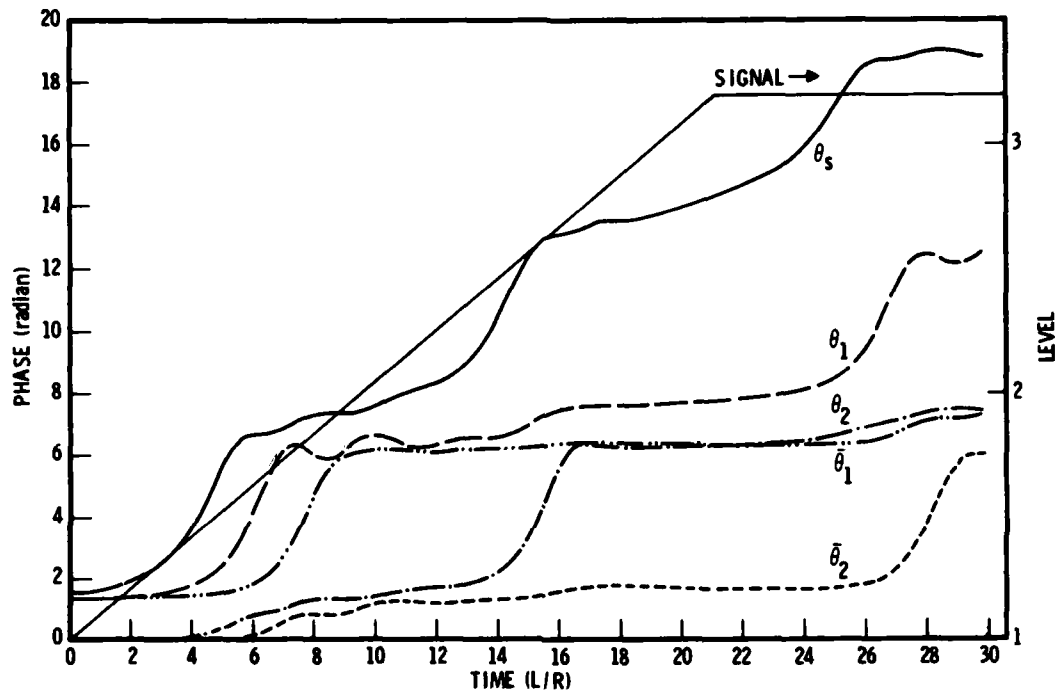


Fig. 11. Simulation Same as in Fig. 9. Response shown in terms of junction phases.

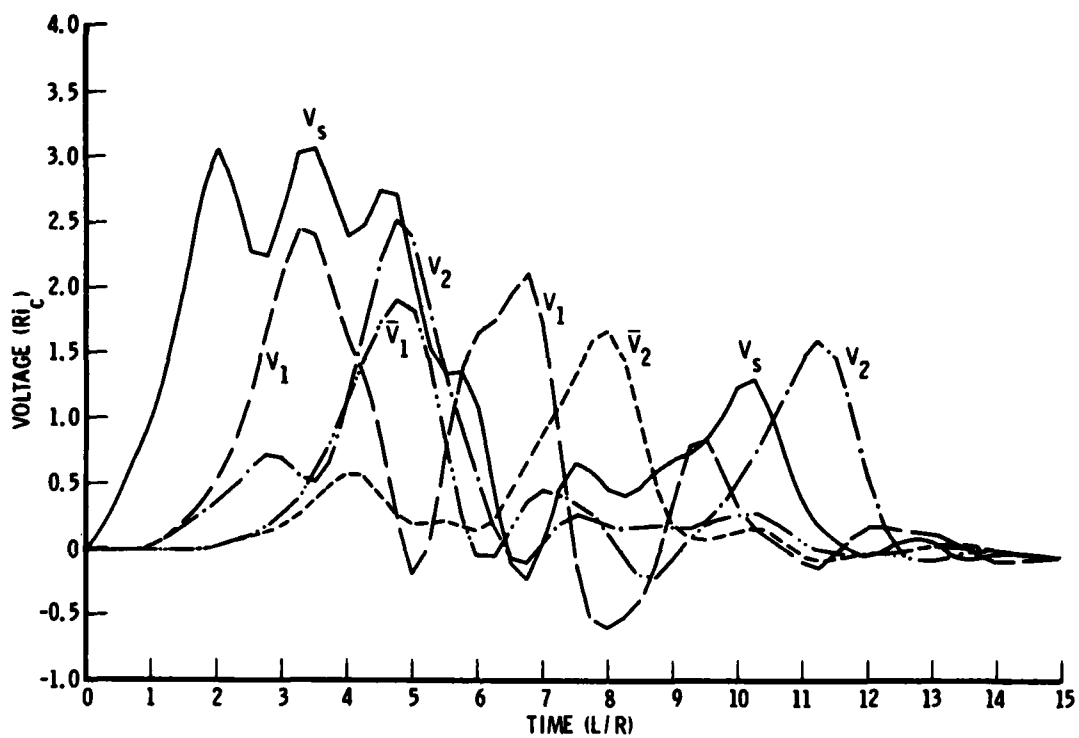


Fig. 12. Simulation Same as in Fig. 9 Except That a Fast Ramp is Used ($I = 2.5 I_c R/L$)

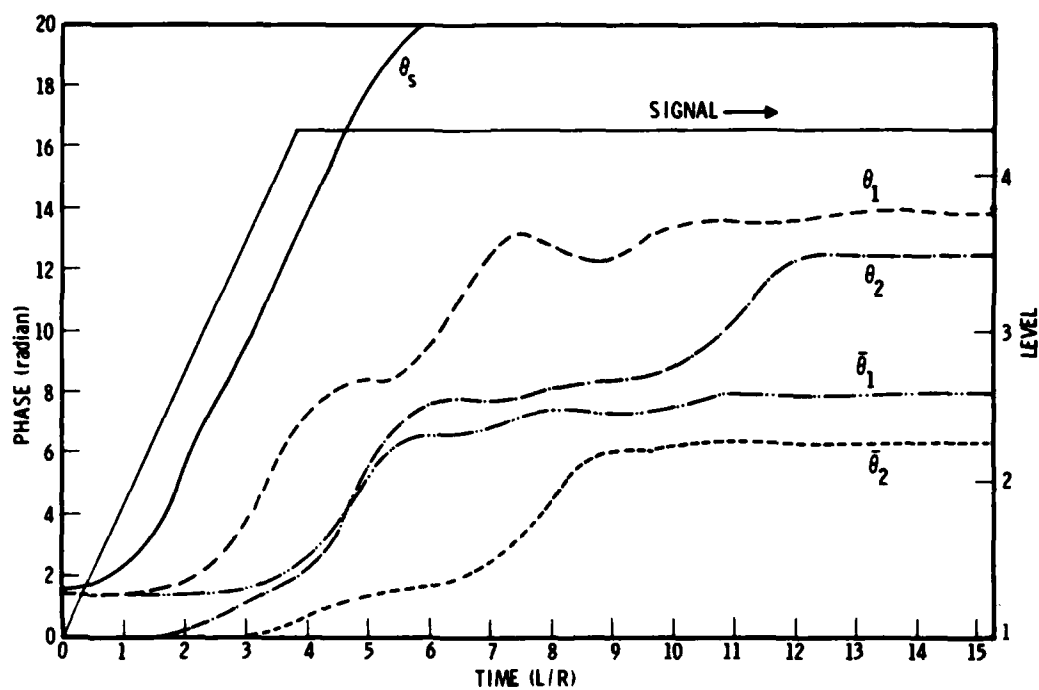


Fig. 13. Simulation Same as in Fig. 12. Response shown in terms of junction phases.

The value of the bias current I_0 affects the gain of the SQUIDs as logic elements. A low value of I_0 can reduce the gain sufficiently such that successive scalars will not switch. A high value results in excessive gain, and false triggering occurs from the reflected signals. The range $0.6 \leq I_0/I_c \leq 0.9$ brackets the useful bias currents for SQUIDs with $\beta = \pi$.

The mutual reflections among the scalar cells deserve more attention. The largest reflection seen in Fig. 10 does not produce a false triggering. This reflection becomes more serious when τ_x is reduced, as in Fig. 9, though even here false triggering does not occur. The issue of inductive loading between the SQUIDs arises because the short sections of microstrip are inductive. When $\tau_x \gg (L/R)$, the SQUID is loaded by Z_x during both the evolution of the pulse and the reflected signal; this prevents excessive ringing in the response. When $\tau_x < (L/R)$, the SQUID becomes loaded by an impedance generated by the succeeding SQUID in series with an inductor $L_x = Z_x \tau_x$. Raising the value of L_x by increasing Z_x increases the magnitude of this ringing, which is insufficiently damped by the resistor $R/2$. Increasing L_x from $0.25 (2L)$ to $(2L)$ fails to induce false triggering, but the settling time is extended as the increase in $(2L_x/R)$ would indicate. Consequently, design of the circuit should try to minimize external inductances where appropriate.

Apart from optimizing β values in the SQUIDs, the ultimate speed of this serial front-end design for an A/D converter is limited by how small (L/R) can be made. For the DJ-SQUIDs, $(L/R) \equiv \beta \phi_0 / 4\pi R I_c = \phi_0 / 4R I_c$ for $\beta = \pi$. Consequently, minimizing (L/R) is equivalent to maximizing the product $R I_c$. When this is performed, the current through the load impedance R will begin to compete with the quasiparticle tunneling in the junctions. This can be accommodated in the simulations by restoring the voltage dependent current $G(\theta)V$ in the tunnel junctions. We have included this term in an elemental, nonrigorous manner by introducing the normal junction resistance R_n above the gap voltage V_g and writing

$$G^{-1}(\theta) = R_n \quad \text{for } V > V_g$$

$$= 10 R_n \quad \text{for } V < V_g$$

$R_n I_c = 0.619 V_g$ for lead tunnel junctions. When R_n becomes comparable to R , extra damping of the junctions occurs and the voltage pulses are clipped. Eventually the gain is reduced sufficiently such that succeeding SQUIDs are not switched by the quantizer. A value $(R_n/R) = 0.5$, which lies close to the minimum acceptable value, has been chosen for the simulation shown in Fig. 14. Writing

$$(L/R) = \frac{\phi_0}{4} \left(\frac{R_n}{R} \right) \left(\frac{1}{R_n I_c} \right) \quad (18)$$

and taking V_g to be 2.4 mV, we find $(L/R) = 2.5 \times 10^{-13} \text{ s}$.

We have considered more than two scaler cells to demonstrate that an extended array of SQUIDs will exhibit correct scaling action. The results for four scaler cells exhibited no unexpected problems.

DESIGN CONSIDERATIONS

We have discussed¹ the design criteria for critically damped SJ-SQUIDs constructed with microstrip technology and Josephson tunnel junctions similar to the IBM technology. The design for $\beta = \pi$ was parametrized in terms of the $(L/2R)$ time constant τ and the flux quantum energy $E \equiv \phi_0^2/2L$. Those results are reproduced in Fig. 15. It was assumed that the junction width w was equal to that of the microstrip, which provided not only the SQUID inductance L but also the loading impedance such that $Z = Z_x = R$. The junction length δ was imposed by the junction capacitance necessary to produce critical damping. Then the current density J was determined by the critical current I_c (controlled by E and β) and the junction area $w\delta$. Smaller junctions can be considered, if overdamping is necessary, by raising the current density and

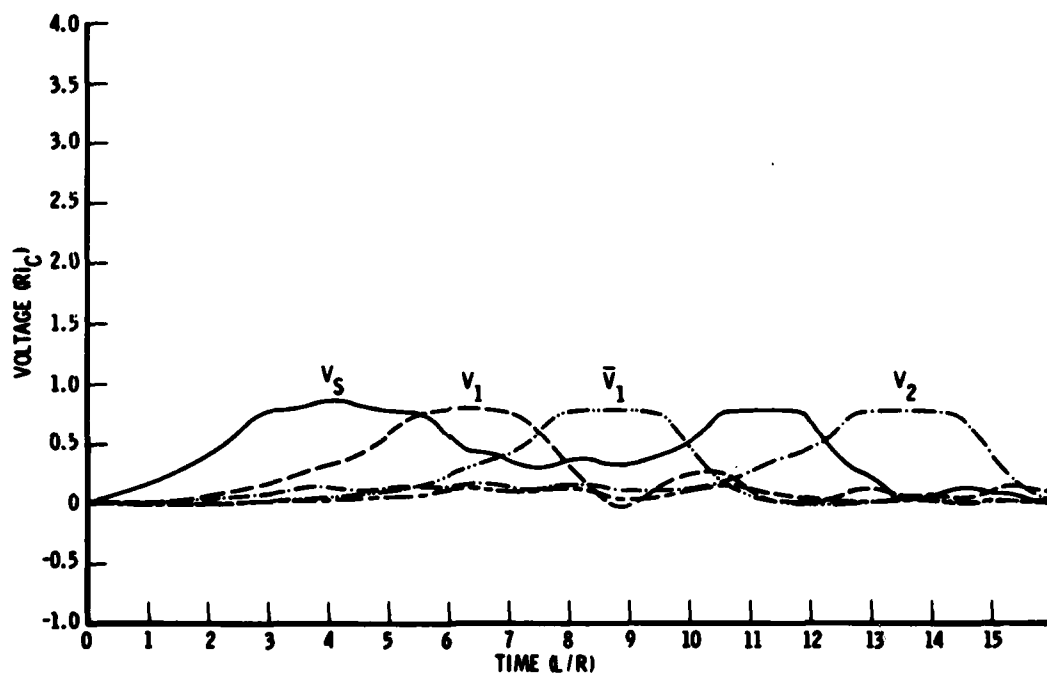


Fig. 14. Simulation to Demonstrate Ultimate Performance.
Ramp speed is $\dot{I} = 0.5 I_C R/L$ and junction shunting
resistance $R_N = 0.5 R$.

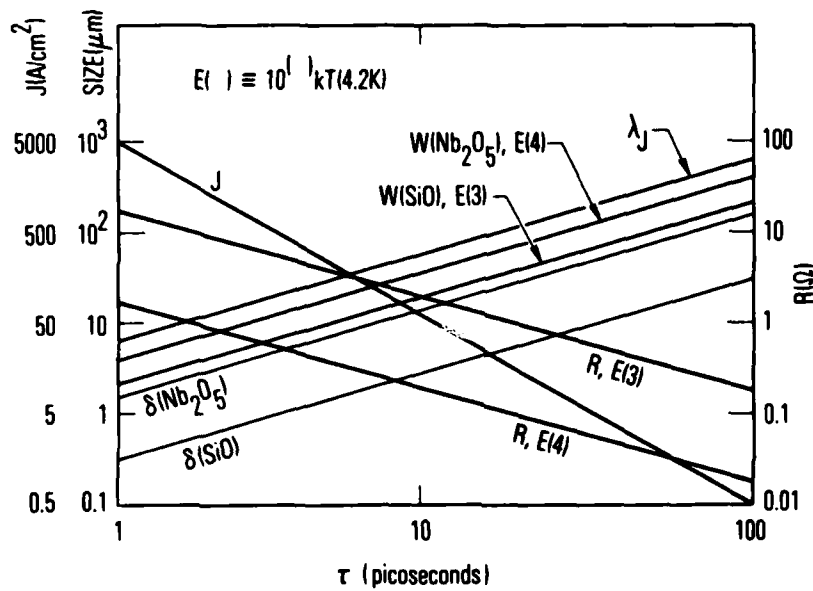


Fig. 15. Design Parameters for a Critically Damped SQUID with β -Value of π . τ represents the switching time $L/2R$.

hence the plasma frequency. Ultimate high speeds, however, require small junctions. Consequently, overdamping merely makes high-speed performance more difficult to achieve. Two microstrip-dielectric-spacer choices were considered: 1500 Å SiO and 500 Å Nb₂O₅.

The energy E was specified in units of $kT(4.2K)$ to demonstrate the relative immunity to thermal noise. Spontaneous switching of the SQUIDs will occur when E is too small. Practical limitations associated with penetration lengths λ_J restrict the maximum value of E .

The need to restrict internal propagation delay within the SQUIDs by lumping L has imposed an impedance requirement of $Z > 4Z_x$. This increased inductance per unit length can be achieved by increasing the dielectric-spacer thickness and/or reducing the effective width of the microstrip. This discontinuity may also generate parasitic inductance, which should be minimized in the external circuit involving the load impedance. Should the need arise for miniaturization, Z may be further increased.

Efficient coupling to the input SQUID is required for weak signals. This can be achieved with a broadband impedance transformation to the micron-sized microstrip. Some filtering is necessary, however, to isolate the fluxoid pulses from the signal. The output from the buffer memory with high clocking rates also requires special attention.

LABORATORY OPERATIONS

The Laboratory Operations of The Aerospace Corporation is conducting experimental and theoretical investigations necessary for the evaluation and application of scientific advances to new military concepts and systems. Versatility and flexibility have been developed to a high degree by the laboratory personnel in dealing with the many problems encountered in the nation's rapidly developing space and missile systems. Expertise in the latest scientific developments is vital to the accomplishment of tasks related to these problems. The laboratories that contribute to this research are:

Aerophysics Laboratory: Launch and reentry aerodynamics, heat transfer, reentry physics, chemical kinetics, structural mechanics, flight dynamics, atmospheric pollution, and high-power gas lasers.

Chemistry and Physics Laboratory: Atmospheric reactions and atmospheric optics, chemical reactions in polluted atmospheres, chemical reactions of excited species in rocket plumes, chemical thermodynamics, plasma and laser-induced reactions, laser chemistry, propulsion chemistry, space vacuum and radiation effects on materials, lubrication and surface phenomena, photo-sensitive materials and sensors, high precision laser ranging, and the application of physics and chemistry to problems of law enforcement and biomedicine.

Electronics Research Laboratory: Electromagnetic theory, devices, and propagation phenomena, including plasma electromagnetics; quantum electronics, lasers, and electro-optics; communication sciences, applied electronics, semiconducting, superconducting, and crystal device physics, optical and acoustical imaging; atmospheric pollution; millimeter wave and far-infrared technology.

Materials Sciences Laboratory: Development of new materials; metal matrix composites and new forms of carbon; test and evaluation of graphite and ceramics in reentry; spacecraft materials and electronic components in nuclear weapons environment; application of fracture mechanics to stress corrosion and fatigue-induced fractures in structural metals.

Space Sciences Laboratory: Atmospheric and ionospheric physics, radiation from the atmosphere, density and composition of the atmosphere, aurorae and airglow; magnetospheric physics, cosmic rays, generation and propagation of plasma waves in the magnetosphere; solar physics, studies of solar magnetic fields; space astronomy, x-ray astronomy; the effects of nuclear explosions, magnetic storms, and solar activity on the earth's atmosphere, ionosphere, and magnetosphere; the effects of optical, electromagnetic, and particulate radiations in space on space systems.

THE AEROSPACE CORPORATION
El Segundo, California

...